PAPER Special Section on Papers Selected from ITC-CSCC 2005

Impact of Timing Jitter on DS-UWB and Hybrid DS-Multiband-UWB Systems with Rake Reception over Multipath Environment

Chin Sean SUM[†a)], ***Student Member***, **Shigenobu SASAKI**[†], ***and*** **Hisakazu KIKUCHI**[†], ***Members***

SUMMARY In this paper, the impact of timing jitter in direct sequence ultra wideband (DS-UWB) system is investigated over multipath fading channel. Also, a novel hybrid direct sequence multiband UWB (DS-MB-UWB) system is proposed to mitigate the impact of timing jitter. We analyze and compare the system performance for conventional DS-UWB and hybrid DS-MB-UWB with Rake receiver in the presence of timing jitter over additive white Gaussian noise (AWGN) and multipath channel. Theoretical framework is developed to calculate the amount of average energy captured in the multipath profiles and symbol error rate (SER) considering the presence of timing jitter. It is found that DS-MB-UWB system, which employs multiple sub-bands is more jitter-robust than conventional DS-UWB systems. Besides, timing jitter is found to have different impacts on DS-UWB and DS-MB-UWB systems corresponding to different parameters such as number of sub-bands employed, pulse shape, center frequency, bandwidth, number of combined paths in Rake receiver and channel power delay profile (PDP). These different impacts are analyzed and discussed in the paper.

key words: *timing jitter, DS-MB-UWB, DS-UWB, Rake reception, SER*

1. Introduction

Ultra wideband (UWB) technology has emerged to be one of the most promising technologies for wireless communications [1], [2]. By using very short pulses typically a few hundred picoseconds to several nanoseconds, UWB system spreads its bandwidth over typically more than 500 MHz [3]. Direct sequence (DS) UWB (DS-UWB) [4] is one of the popular UWB modulation methods, which is able to offer advantages such as better multipath resolvability [5] and robustness to multi user interference [6]. All these features have enabled DS-UWB technology to be applied in high speed and short range communication, and therefore, a suitable candidate for wireless personal area network (WPAN) [7].

Since short pulse waveform is employed in UWB systems, timing jitter in pulse generator and other devices would have a more significant impact to the system performance as compared to various conventional wireless communication systems. UWB signal pulse design in the order of several-nanosecond duration has to take into consideration at least timing jitter in the order of 10ps achievable only by recently reported clock accuracy [8], [9]. Sensitivity towards timing jitter increases correspondingly if pulse duration is decreased to meet various design demands [10].

Recently, several studies have been reported on the impact of timing jitter. Works in [11], [12] investigated the timing error tolerances for time hopping (TH) UWB systems. Work in [13] reported that different types of Rake receivers are subjected to different impacts by timing jitter. The different impact of timing jitter on various modulation techniques such as orthogonal pulse position modulation (PPM), optimum PPM, binary phase shift keying (BPSK) and on-off keying (OOK) in UWB impulse radio are investigated in [14]. Impact of timing jitter in TH-UWB system under multi-user environment is considered in [15]. Most of these studies are based on classical TH-UWB system. However, in DS-UWB system, the impact of timing jitter has not been given as much attention.

In this paper, the impact of timing jitter in DS-UWB system is investigated. Also, we propose a novel hybrid direct sequence multiband (DS-MB) UWB system that is able to outperform conventional DS-UWB systems in the presence of timing jitter. DS-MB-UWB system occupies a few narrower sub-bands instead of a wider single band, and therefore, employs longer pulse waveforms. In our analysis, we show how the employment of longer pulses in DS-MB-UWB system reduces the performance degradation caused by timing jitter. There are existing literatures reporting methods of mitigating the impact of timing jitter in UWB systems by manipulating different pulse shapes [16] and different Rake receivers [13], [17], but to the best knowledge of the authors, employing multiple sub-bands to achieve better system performance in timing jitter environment has not been explored.

Also, analysis and comparison is conducted between conventional DS-UWB systems and the proposed DS-MB-UWB system corresponding to parameters such as number of employed sub-bands, pulse shape, center frequency, occupied bandwidth, number of combined paths in Rake receiver and channel power delay profile (PDP). Despite its popularity, performance analysis for DS-UWB system in the presence of timing jitter has not been given much attention as compared to TH-UWB system and is therefore, of interest to the UWB community.

The organization of this paper is as follows. Sec-

Manuscript received September 8, 2005.
Manuscript revised December 30, 2005.
Final manuscript received February 13, 2006.

[†]The authors are with the Department of Electrical and Electronic Engineering, Niigata University, Niigata-shi, 950-2181 Japan.
a) E-mail: sum@telecom0.eng.niigata-u.ac.jp

DOI: 10.1093/ietfec/e89–a.6.1657

tion 2 describes the system model of DS-UWB and DS-MB-UWB over AWGN and multipath channel with Rayleigh distributed fading in the presence of timing jitter. Section 3 presents framework developed to analyze the system performance in jitter environment. Next, Sect. 4 presents numerical analysis with specific examples and discussions concerning the energy capture behavior and SER performance. Finally concluding remarks and future works are presented.

2. System Models

2.1 Signal Model

We consider an M-ary phase shift keying (MPSK) for both DS-UWB and DS-MB-UWB systems as shown in Fig. 1. The general representation of the transmitted signal is given by:

$$s(t) = A \sum_{i=-\infty}^{\infty} \sum_{j=0}^{N_s-1} \cos \phi_i c_j w(t - iT_s - jT_c) \cdot \cos 2\pi f_m (t - jT_c) \quad (1)$$

where

- A = pulse amplitude.
- N_s = number of DS chips per symbol.
- c_j = direct sequence pseudorandom noise (PN) code.
- T_s = symbol duration.
- T_c = chip duration.
- $w(t)$ = shape of the transmitted pulse.
- ϕ_i = $\{q(2\pi/M), q = 0, 1, ..., M-1\}$. = transmitted M-ary phase.
- M = M-ary signaling level.
- f_m = multiband center frequency selected from $m = \{1, 2, 3, ..., B\}$.
- B = total number of employed sub-bands in DS-MB-UWB system.

The transmitted signal in (1) is a DS-MB-UWB signal employing B sub-bands. The MPSK data is spread by N_s chips each with center frequency f_m. The center frequency is constantly hopping from one sub-band to another, chosen from the total B sub-bands. The sub-bands are spectrally orthogonal towards each other. The multiband frequency hopping rate S_r, or how frequent the changing of f_m is, can be expressed by $1/T_c$. This means that the hopping of multiple sub-bands is synchronized with the transition of the DS chips. One DS chip is modulated with one center frequency, then the next chip with a different center frequency, and so on. The sub-band bandwidth and total bandwidth can be defined as $2/T_c$ and $2B/T_c$ respectively. At the receiver side, DS chips with the same polarity and multiband center frequency as the corresponding transmitted signal are used as the template signal for correlation process. In other words, it is assumed that the receiver has knowledge of the DS chip sequence and frequency hopping pattern of the transmitter.

Next, we can easily modify (1) to describe different types of data modulation. For DS-UWB system with a constant center frequency, we set B=1 and f_m=f_c where f_c is the center frequency. Here, the bandwidth is also defined as $2/T_c$. If a baseband UWB pulse is used, we set f_m=0 so that the expression $\cos 2\pi f_m(t - jT_c)$ in (1) becomes 1. The bandwidth is then defined as $1/T_c$.

Here we note that the data rate R for all systems can be defined as $1/T_s$. Also, the chip duty factor δ is defined as T_p/T_c where T_p is the pulse duration, $T_p \le T_c$ and $\delta \le 1$.

Figures 2 and 3 illustrates the spectral and signaling diagrams for the systems. Figure 2 shows how the multiple sub-bands of DS-MB-UWB are spectrally placed as compared to DS-UWB systems. In Fig. 3, we show the different signaling diagrams for conventional DS-UWB and DS-MB-UWB systems. For a DS-UWB signal using baseband pulse waveform as illustrated in Fig. 3(a), we assume a BPSK data with polarity 1 (noted as 'data' in Fig. 3) that is spread by N_s baseband chip waveforms (in Fig. 3(a), N_s=7) with polarity uniformly distributed on $\{+1, -1\}$ (noted as 'chips' in Fig. 3). This can be illustrated by referring to $s_1(t)$ in Fig. 3(a). The polarity for $s_1(t)$ will be the opposite if the BPSK data has a polarity of -1. In DS-UWB signal using pulse waveform with a constant center frequency as illustrated by $s_2(t)$ in Fig. 3(b), cosine wave with frequency f_c (noted as 'center frequency f_c') is modulated into each spreading chips and then into the BPSK data. And for the DS-MB-UWB signal, the center frequency selected from a total number of B frequencies (in Fig. 3(c), B=3) are modulated into the chips at the rate S_r and then into the BPSK data. The transmitted signal can be illustrated by $s_3(t)$ in Fig. 3(c).

Over an AWGN and multipath channel with Rayleigh distributed fading, the received signal can be described as:

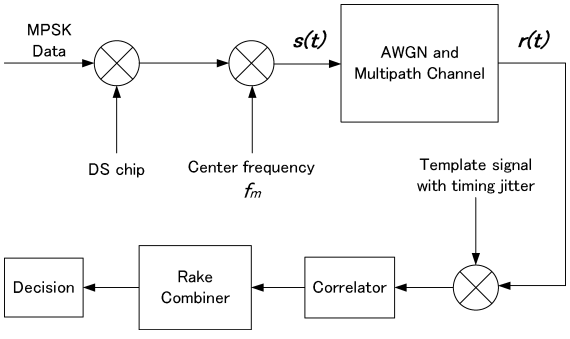

Fig. 1 System diagram of DS-UWB and DS-MB-UWB system.

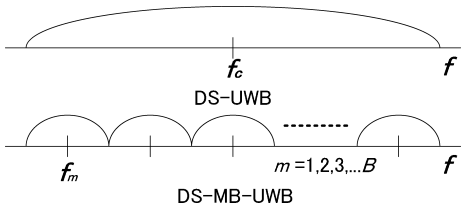

Fig. 2 Spectral diagram for DS-UWB and DS-MB-UWB systems.

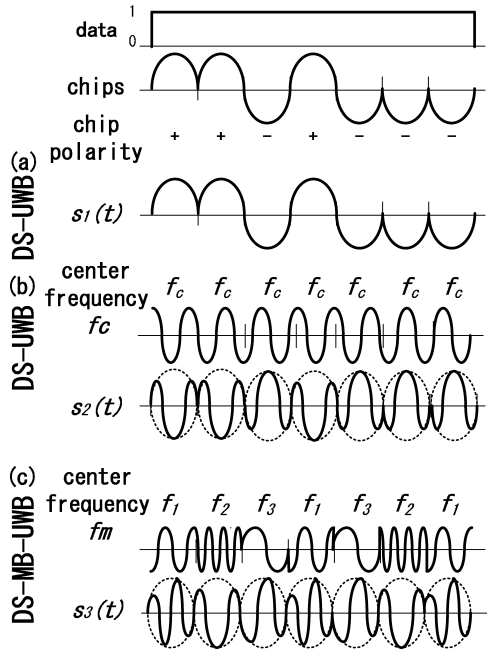

Fig. 3 Signaling diagrams for DS-UWB and DS-MB-UWB systems. (a) DS-UWB signal using baseband pulse waveform, (b) DS-UWB signal using pulse waveform with center frequency f_c and (c) DS-MB-UWB signal.

$$\begin{aligned} r(t) &= s(t) * h(t) + \eta(t) \\ &= A \sum_{i=-\infty}^{\infty} \sum_{j=0}^{N_s-1} \cos\phi_i c_j v(t - iT_s - jT_c) \\ &\qquad \cdot \cos 2\pi f_m (t - jT_c) + \eta(t) \end{aligned} \tag{2}$$

where

$h(t)$ = the channel impulse response.
$\eta(t)$ = white Gaussian noise.
$v(t)$ = channel response of the signal, $v(t) = w(t) * h(t)$
$*$ = convolution process.

Here, we assume the channel to have a maximum delay spread T_d with respect to the first arriving path and $T_d \leq T_c$ so that interchip interference can be negligible. The total number of resolvable multipath is given by $L = T_d/T_p$. Also, our system is assumed to have a sufficiently long PN code that is able to maintain orthogonality between adjacent symbols.

2.2 Receiver Model

The received signal is a series of energy present in the multiple arriving paths at delays with respect to the first arriving path. By using multiple Rake fingers, the correlator correlates the received signal at multiple delays with a template signal to capture the energy from that particular path. Then the Rake combiner combines the captured paths to form the decision statistic. We assume the receiver to have knowledge of the phase and amplitude of each path of the received signal.

The normalized template signal used in the receiver can be given by:

$$\varphi(t) = \frac{1}{\sqrt{N_s}} \sum_{j=0}^{N_s-1} c_j w(t - jT_c) \cos 2\pi f_m (t - jT_c) \tag{3}$$

$$m = 1, 2, 3..., B$$

The correlation process between the received signal $r(t)$ at the l-th Rake finger with delay τ_l and the template signal $\varphi(t)$ with an instantaneous timing jitter ϵ_l, can be described by:

$$Z_l = \int_0^{T_s} r(t)\varphi(t - \tau_l - \epsilon_l)dt = \alpha_l \chi(\tau_l + \epsilon_l) + \eta_l \tag{4}$$

where

η_l $= \int_0^{T_s} \eta(t)\varphi(t)dt.$
$\chi(t)$ $= \int_0^{T_s} v(t)\varphi(t - \tau_l - \epsilon_l)dt$ is the cross correlation function between channel response and template signal.
α_l = signal amplitude of the l-th path.

Next, the Rake combiner with maximal ratio combining (MRC) method [18] combines the best selected L_c paths out of the total resolvable L paths to form the decision statistic:

$$Z = \sum_{l=1}^{L_c-1} \alpha_l \chi(\tau_l) Z_l + \eta = \sum_{l=1}^{L_c-1} \alpha_l^2 \chi(\tau_l)\chi(\tau_l + \epsilon_l) + \eta \tag{5}$$

where $\eta = \sum_{l=1}^{L_c-1} \alpha_l \chi(\tau_l)\eta_l$.

Here we note that a selective Rake (SRake) selects $L_c < L$ best paths to be combined, whereas an all Rake (ARake) combines all L paths. Compared to ARake, SRake is reported to be more practical for UWB systems [19] and is therefore applied in this paper.

2.3 Channel Model

With the channel models, we describe the pattern of how the energy in the received signal is distributed along the multipaths. Firstly, the received signal amplitudes at a certain path are assumed to follow the Rayleigh fading distribution. The mean value of these Rayleigh faded signals give the average energy present at that particular path. In this paper, the distribution pattern of average energy along the multipath profile is defined by flat and exponentially decaying power delay profile (PDP). Both PDP's have the same amount of total energy. As shown in Fig. 4, for a flat PDP, the distribution of the average energy (which can also be expressed as the average signal to noise ratio (SNR)) is uniform along all L paths. As for an exponentially decaying PDP, the first path has the biggest portion of average SNR, and for the following paths the SNR decreases in an exponential manner.

For a flat PDP, the average SNR for each path is:

$$\gamma_l = \Gamma \mathrm{E}[\alpha_l^2] = \frac{\Gamma}{L}, l = 1, 2, 3, ..., L \tag{6}$$

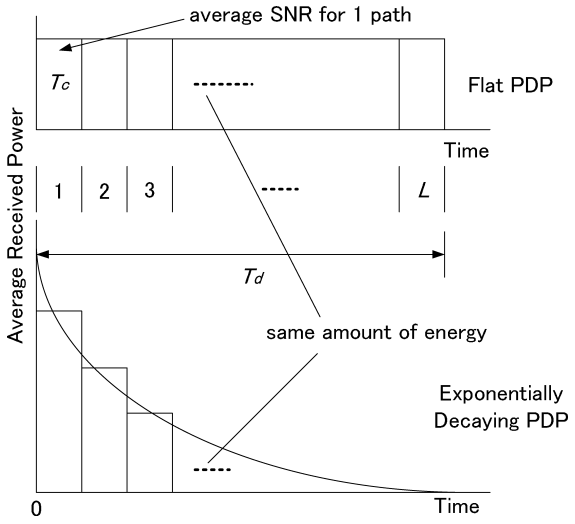

Fig. 4 Flat and exponentially decaying PDP.

where

Γ = system SNR, $\Gamma = E_s/N_0$.
E_s = symbol energy, $E_s = N_s A E_p$.
N_0 = noise power.
E_p = pulse energy.
E[·] = mean value of [·].

As for an exponential decaying PDP, the average SNR for each path can be given by [20]:

$$\gamma_l = \Gamma\left[\frac{1-\exp(-C/L)}{1-\exp(-C)}\right]e^{-C[\frac{l-1}{L}]} \qquad C > 0, 1, 2, ..., L \tag{7}$$

where C denotes the representation of the decaying rate of the average path SNR [21]. At different values of C, the energy distribution pattern versus time will be different, but the total amount of energy in the channel response remains the same. For larger C values, most energy are concentrated at the earlier period of time and decaying process takes place more rapidly.

3. Performance Analysis

In this section, by using the system models presented in the previous section, we develop the theoretical framework to analyze the system performance in the presence of timing jitter.

3.1 Autocorrelation Property

In the presence of timing jitter, pulse shape is one of the major factors affecting the average energy able to be captured by the Rake receiver and the overall system performance. Here, we consider two types of commonly used pulses, the monocycle pulse and the modulated Gaussian pulse. Monocycle pulse [19], often employed in the UWB impulse radio [22], [23] is used for the DS-UWB systems in this paper. The modulated Gaussian pulse [10], that is able to modulate the system to higher center frequency, is used for both DS-UWB and DS-MB-UWB systems in this paper.

The monocycle pulse can be described as:

$$w(t) = \left(1 - 4\pi\left(\frac{t}{t_{pc}}\right)^2\right)\exp\left(-2\pi\left(\frac{t}{t_{pc}}\right)^2\right) \tag{8}$$

where $t_{pc} = 0.39T_p$ [19], [24] is the pulse width constant and T_p is the pulse duration. The autocorrelation function of the monocycle pulse with an instantaneous timing jitter ϵ and normalized to the pulse energy, can be given as:

$$\begin{aligned} G(\epsilon) &= \frac{\int_{-\infty}^{\infty} w(t)w(t-\epsilon)dt}{\int_{-\infty}^{\infty} w^2(t)dt} \\ &= \frac{4}{3}\exp\left(\frac{-\alpha\epsilon^2}{4}\right)\left(\frac{\alpha^2\epsilon^4}{16} - \frac{3\alpha\epsilon^2}{4} - \frac{3}{4}\right) \end{aligned} \tag{9}$$

where $\alpha = 4\pi/t_{pc}^2$.

As for the modulated Gaussian pulse, the pulse equation can be derived as:

$$w(t) = \cos(2\pi f_m t)\exp\left(-2\pi\left(\frac{t}{t_{pc}}\right)^2\right) \tag{10}$$

And the autocorrelation function normalized to the pulse energy can be given as:

$$G(\epsilon) = \cos(2\pi \cdot \mathrm{E}[f_m] \cdot \epsilon)\exp\left(\frac{-\pi\epsilon^2}{t_{pc}^2}\right) \qquad m = 1, 2, 3, ..., B \tag{11}$$

where f_m is the multiband center frequency and B is the total number of employed sub-bands for DS-MB-UWB system. E[fm] denotes the mean value of the multiband center frequencies. And for a DS-UWB system, $f_m = f_c$ and B=1. Additionally, it is worth noting that $G(\epsilon)$ means the ratio between the correlator output in the presence of instantaneous timing jitter ϵ, and the correlator output without timing jitter.

3.2 Timing Jitter Model

To characterize the timing jitter present in the template signal generator, Gaussian distribution is assumed. The reason is, in most electrical circuits, thermal noise that causes timing error is Gaussian distributed. And if there are several uncorrelated composite effects with different distributions that cause the timing error to occur, these effects approach Gaussian distribution, according to the central limit theorem [25].

First of all, we describe the Gaussian probability density function (PDF):

$$\psi(\epsilon) = \frac{1}{\sigma\sqrt{2\pi}}\exp\left(\frac{-\epsilon^2}{2\sigma^2}\right) \tag{12}$$

where σ is the standard deviation of the distribution.

Thus, the pulse autocorrelation function in the presence of a Gaussian distributed timing jitter having a standard deviation σ can be described as:

For monocycle pulse,

$$G(\sigma) = \left(\frac{1}{\sigma\sqrt{2}}\right)\left(\frac{\pi^2}{t_{pc}^4\left(\sqrt{\frac{\pi}{t_{pc}^2}+\frac{1}{2\sigma^2}}\right)^5} - \frac{2\pi}{t_{pc}^2\left(\sqrt{\frac{\pi}{t_{pc}^2}+\frac{1}{2\sigma^2}}\right)^3} + \frac{1}{\left(\sqrt{\frac{\pi}{t_{pc}^2}+\frac{1}{2\sigma^2}}\right)}\right) \tag{14}$$

And for modulated Gaussian pulse,

$$G(\sigma) = \left(\frac{1}{\sigma\sqrt{2}}\right)\left(\frac{1}{\sqrt{\frac{\pi}{t_{pc}^2}+\frac{1}{2\sigma^2}}}\right)\exp\left(\frac{-\pi^2\mathrm{E}[f_m]^2}{\sqrt{\frac{\pi}{t_{pc}^2}+\frac{1}{2\sigma^2}}}\right), \quad m = 1, 2, 3, ..., B \tag{15}$$

$$G(\sigma) = \int_{-\infty}^{\infty} G(\epsilon)\psi(\epsilon)d\epsilon \tag{13}$$

For different pulse shapes, $G(\sigma)$ is expressed differently as given in Eqs. (14) and (15) in the top of this page. In (14) and (15), the timing jitter standard deviation σ is described as the root mean square jitter (RMSJ) and is expressed in nanoseconds or picoseconds.

3.3 Average Captured Energy in Jitter Environment

The amount of energy captured from the multipath is determined by the correlator output. With a jitter-free correlator output, we assume that the energy from each path can be fully captured by the Rake receiver. However, with the presence of timing jitter, the mistiming of the template signal causes the captured energy to decrease considerably, thus affecting system performance.

In this section, we develop the calculation for average energy that is able to be captured by the Rake receiver in the presence of a Gaussian distributed timing jitter. The correlation between a single pulse of the jittered template signal and the received pulse produces the correlator output that can be given by:

$$x_m = \int w(t)w(t+\sigma)dt = E_p G(\sigma) \tag{16}$$

And the variance of the correlation of the jittered template pulse signal with noise can be described as:

$$x_v^2 = \mathrm{E}\left[\left(\int \eta(t)w(t+\sigma)dt\right)^2\right] = N_0 E_p \tag{17}$$

Using (16) and (17), considering the effects of N_s and A, the total SNR for a received symbol in the presence of Gaussian distributed jitter can be given as:

$$\Gamma_j = \frac{N_s A x_m^2}{x_v^2} = \frac{E_s}{N_0}G(\sigma)^2 \tag{18}$$

Therefore, referring to the average SNR γ_l in each path as described in (6) for flat PDP and (7) for exponentially decaying PDP, the average energy able to be captured by the Rake receiver at the l-th path in the presence of Gaussian distributed timing jitter can be described as:

For flat PDP,

$$\beta_l = E_s G(\sigma)^2 E[\alpha_l^2] = \frac{E_s G(\alpha)^2}{L}, l = 1, 2, ..., L \tag{19}$$

For exponentially decaying PDP,

$$\beta_l = E_s G(\sigma)^2 \left[\frac{1-\exp(-C/L)}{1-\exp(-C)}\right] e^{-C\left(\frac{l-1}{L}\right)} \quad C > 0, l = 1, 2, ..., L \tag{20}$$

where $\mathrm{E}[\cdot]$ denotes the mean value of $[\cdot]$.

3.4 Symbol Error Probability

The average energy captured and combined from the multipath determines the system performance. With the presence of timing jitter, the average energy capture decreases and thus degrades the SER performance. For analysis of system performance of the DS-UWB and DS-MB-UWB systems with SRake in the presence of Gaussian distributed timing jitter over AWGN and multipath channel with Rayleigh distributed fading with a given PDP, we describe the system SER [26] as:

$$SER_{SRake} = \frac{1}{\pi}\int_0^{\Theta}\prod_{l=1}^{L_c}\left[\frac{\sin^2(\theta)}{\lambda_{MPSK}\gamma_l G(\sigma)^2 + \sin^2(\theta)}\right] \cdot \prod_{l=L_c+1}^{L}\left[\frac{\sin^2(\theta)}{\lambda_{MPSK}\gamma_l G(\sigma)^2\frac{L_c}{l} + \sin^2(\theta)}\right] d\theta \tag{21}$$

where

γ_l = average SNR in the l-th path.
L_c = number of selected and combined paths out of the L number of total resolvable paths.
λ_{MPSK} = $\sin^2(\pi/M)$.
Θ = $\pi(M-1)/M$.
M = M-ary signaling level.

4. Numerical Examples and Discussions

Based on the theoretical framework developed in the previous section, the performance of the DS-UWB and DS-MB-UWB systems are evaluated numerically. The impact

of timing jitter is evaluated based on the aspects of pulse waveform, data modulation, center frequency, bandwidth, employed bands, Rake reception, types of channel and M-ary signaling level. The chip duty factor δ is set to unity for this analysis. Also, the interchip interference is assumed to be negligible.

4.1 Pulse Waveform

DS-UWB system performance in the presence of timing jitter is affected by pulse waveform because the pulse autocorrelation function determines the fraction of energy that can be captured by the receiver. In this analysis we compare the difference of using a baseband monocycle pulse, as given in (8) to a modulated Gaussian pulse with a center frequency, as given in (10). Normalized RMSJ (NRMSJ) is used to express the timing jitter. NRMSJ is defined as the ratio of RMSJ over pulse duration T_p and is quantified in percentage (%). Different NRMSJ have different impact on the pulse autocorrelation function as given in (13), thus having different amount of captured energy as given in (19) and (20). By considering these parameters, the system BER performance can be determined by applying (21).

In Fig. 5, we show the BER performance of DS-UWB systems employing monocycle pulse and modulated Gaussian pulse. For both systems, L_c=4 paths are combined. The maximum delay spread T_d is 100 ns. Signal bandwidth BW and SNR are set to be 2 GHz and 15 dB respectively. Also, both systems employ binary phase shift keying (BPSK) modulation and multipath channel with Rayleigh distributed fading and exponentially decaying PDP and C=10. Since BPSK is employed, system performance is expressed by bit error rate (BER) instead of SER. Without timing jitter, BER performance for both pulse waveforms is similar. As NRMSJ increases, performance degradation can be observed for both pulse waveforms. However, the degradation rate of the modulated Gaussian pulse is more rapid than the monocycle pulse. For the monocycle pulse, the total NRMSJ that degrades the system to BER of 10^{-1} is approximately 20% of the pulse duration, whereas for modulated Gaussian pulse, the NRMSJ as low as 2% of the pulse duration will degrade the system to BER of 10^{-1}. Additionally, modulated Gaussian pulse with a lower center frequency performs better than high center frequency.

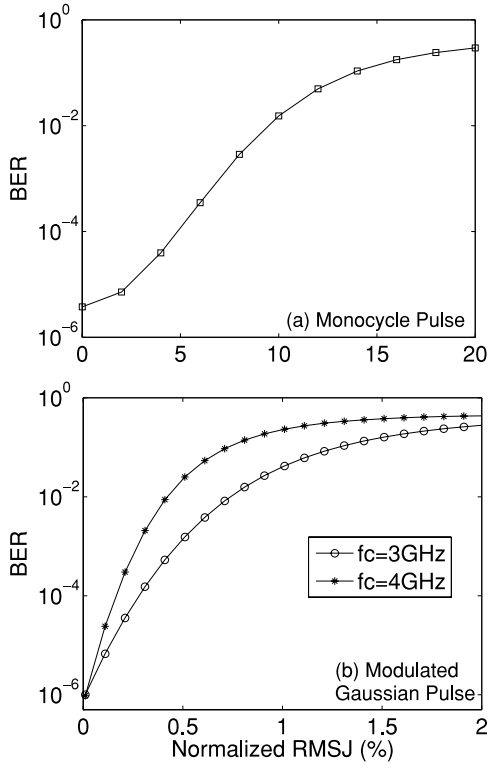

Fig. 5 BER performance vs. NRMSJ for Pulses (a) Monocycle and (b) Modulated Gaussian. BW=2 GHz, SNR=15 dB, L_c=4, T_d=100 ns, BPSK, Exp. decaying PDP, C=10.

The results in Fig. 5 can be explained by referring to the energy capture achievable by different pulse waveforms as shown in Fig. 6. Without timing jitter, no difference in the amount of energy captured is observed for both pulses. However, as NRMSJ increases, amount of captured energy decrease differently according to different pulse waveforms. The amount of energy captured by modulated Gaussian pulse decreases more rapidly as compared to monocycle pulse. For monocycle pulse, at NRMSJ=6%, the energy decreases half of the total amount of energy, whereas for modulated Gaussian pulse, the energy decreases to half at as low as NRMSJ=1%. The captured energy by modulated Gaussian pulse approaches 0% at NRMSJ> 6%. Here it is also worth noting that the modulated Gaussian pulse with lower center frequency outperforms those with higher center frequency. The different energy capture behavior of different pulse waveforms can be explained by respective pulse autocorrelation function, which determines the correlator output of the receiver. The autocorrelation function of the modulated Gaussian pulse decreases more rapidly as compared to monocycle pulse, thus having less captured energy as NRMSJ increases.

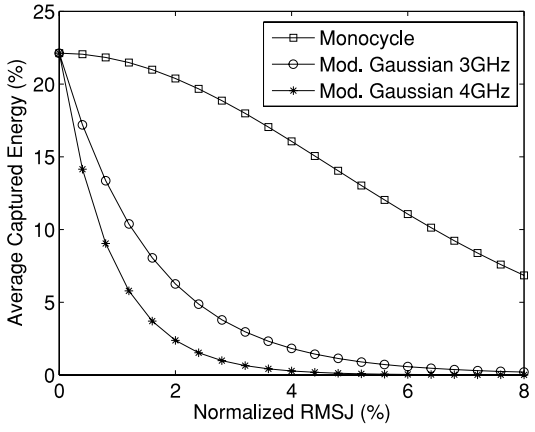

Fig. 6 Average captured energy vs. NRMSJ for different pulse waveforms. T_p=0.25 ns, L=40, L_c=4, BPSK, Exp. decaying PDP, C=10.

4.2 Center Frequency and Bandwidth

In DS-UWB system with constant center frequency, frequency f_c and bandwidth BW are two main factors affecting the amount of captured energy and BER performance in timing jitter environment. For the modulated Gaussian pulse as given in (10), different f_c and BW changes the pulse autocorrelation function as in (13), and thus affect the amount of energy captured as described by (19) and (20). The discussion on energy capture corresponding f_c and BW can be found referring to Fig. 8 and Fig. 10 respectively. As a result of different energy capture, the BER performance as given in (21) can be determined. Figures 7 and 9 discusses the different BER performance.

The BER performance due to varying f_c is presented in Fig. 7. System parameters such as SNR, T_d and L_c are set to be 20 dB, 80 ns and 4 respectively. To modulate the system with different center frequency, modulated Gaussian pulse is employed. For BW=1 GHz, we found that as f_c increases, the system BER performance degrades. On the other hand, for BW=4 GHz, BER performance improves when f_c increases from 3.1 to 5 GHz, but then degrades if f_c continues to increase beyond 5 GHz. This shows increasing f_c generally degrades BER performance, except for system with higher BW, where increasing f_c at lower frequency range improves BER performance. Additionally, with the presence of higher NRMSJ, system performance degrades more rapidly and saturates to a certain BER.

Next, Fig. 8 is used to explain the results observed in Fig. 7. For BW<2 GHz, captured energy generally decreases as f_c increases. We are aware that the less energy captured by the receiver, the more severely BER performance will be degraded. This explains the results for solid lines in Fig. 7. However, if BW goes beyond 2 GHz, achievable energy capture at lower f_c becomes less if higher BW is employed. Besides, when f_c increases, captured energy increases slightly but beyond a certain f_c, it decrease con-

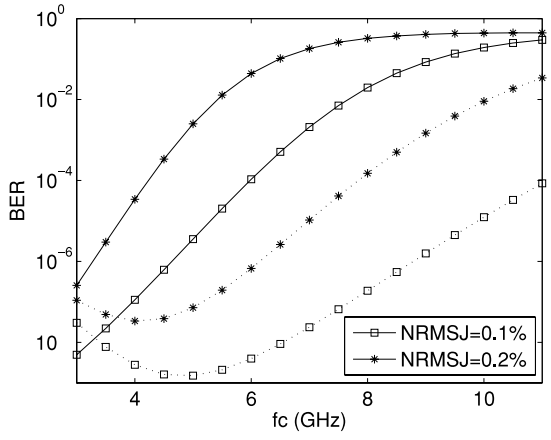

Fig. 7 BER performance vs. center frequency for DS-UWB system. T_d =80 ns, L_c=4, SNR=20 dB, BPSK, Exp. decaying PDP, C=10, modulated Gaussian pulse. Solid line: BW=1 GHz, Dotted line: BW=4 GHz.

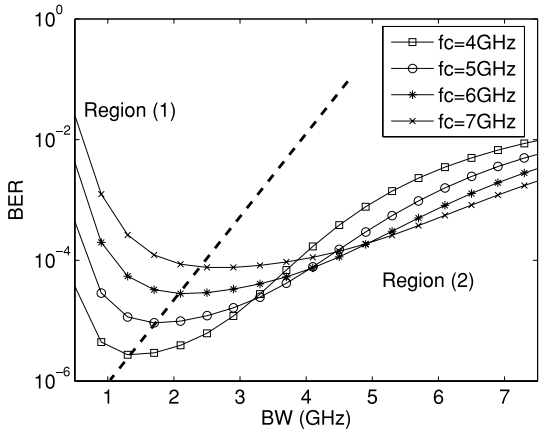

Fig. 9 BER performance vs. bandwidth for DS-UWB system. T_d = 100 ns, L_c=10, NRMSJ=0.1%, SNR=16 dB, BPSK, Exp. decaying PDP, C=10.

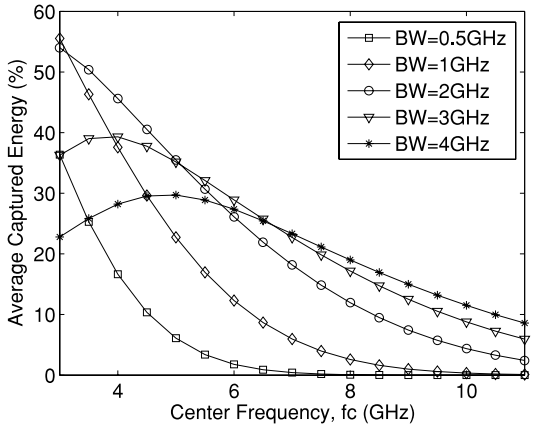

Fig. 8 Average captured energy vs. center frequency for DS-UWB system. NRMSJ=0.1%, T_d=80 ns, L_c=10, BPSK, Exp. decaying PDP, C=10.

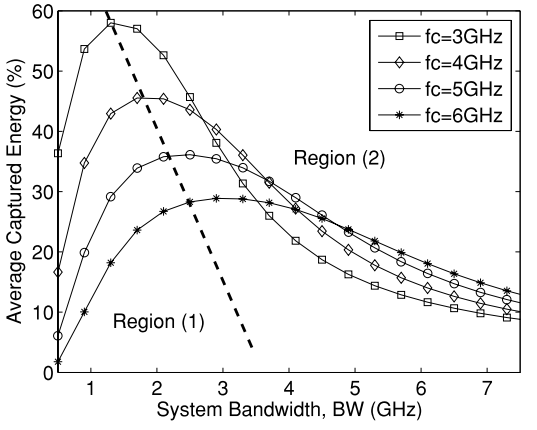

Fig. 10 Average captured energy vs. bandwidth for DS-UWB system. NRMSJ=0.1%, T_d=80 ns, L_c=10, BPSK, Exp. decaying PDP, C=10.

siderably. This explains the BER performance behavior of the dotted lines shown in Fig. 7.

Figure 9 illustrates the BER performance for varying BW. For clearer elaboration, Fig. 9 is divided into region 1 and 2. In region 1, as BW increases, BER performance improves to a certain point. In this region, systems with lower f_c are found to perform better. In region 2, as BW continues to increase, BER performance on the other hand, starts to degrade. In this region, it is observed that systems employing lower f_c degrade more rapidly. The division of region 1 and 2 suggests that an optimum point exists for DS-UWB system with varying BW.

Figure 10 shows the energy capture for DS-UWB system with varying BW. In region 1, as BW increases, more energy can be captured generally. Comparatively, systems with lower f_c are able to capture more energy. However, in region 2, as BW continues to increase, the captured energy decreases. Also, in this region, captured energy for systems with lower f_c is found to decrease more rapidly.

4.3 Data Modulation and Number of Bands

The analysis in Sect. 4.2 has shown that for DS-UWB systems, BW is an important parameter to determine the impact of timing jitter. So, instead of using short pulses to occupy a single wide bandwidth, we can divide the total bandwidth into several narrower sub-bands, and thus using longer pulses. By using longer pulses, system tolerance against timing jitter can be increased. Additionally, the employment of longer pulses enables more fractional energy to be captured by template signal in the receiver. This will improve system performance in timing jitter environment. Therefore, in this section, we propose the novel DS-MB-UWB system that employs multiple narrow sub-bands to explore this potential.

Referring to the results shown in Fig. 9, the optimum BW separates the DS-UWB system into two regions: region 1 where increasing BW improves BER performance and region 2 where increasing BW degrades BER performance. We are aware that in region 2, using smaller BW gives us better BER performance. Manipulating this knowledge, we assign multiple narrower sub-bands in region 2 to the system instead of using a wider single band. As long as the employed BW for the sub-bands fall in region 2, we know that as BW decreases, BER performance improves. The total bandwidth of all the sub-bands is equivalent to the single band bandwidth. The rest of this section will show how the proposed DS-MB-UWB outperforms DS-UWB systems in timing jitter environment.

The DS-MB-UWB signal with B sub-bands is given by (1). Using longer pulses affects the pulse autocorrelation function given in (13) since pulse correlation function is dependent on pulse duration. Therefore, by transmitting signal with different system SNR as given in (6) and (7), and by having different pulse autocorrelation function in the presence of timing jitter, the average SNR of the received symbol changes accordingly, as described in (18). As a result, the amount of captured energy can be obtained by applying (19) and (20). Finally, BER performance can be determined according to (21).

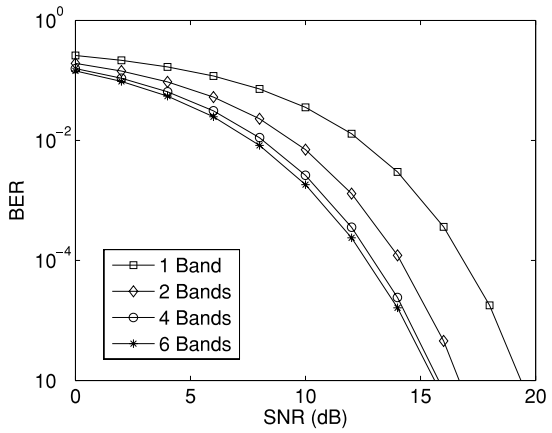

Fig. 11 BER performance vs. SNR for DS-UWB and DS-MB-UWB systems. T_d=200 ns, L_c=4, BW=6 GHz, NRMSJ=0.01%, BPSK, Exp. decaying PDP, C=10.

Figure 11 presents the BER performance for DS-MB-UWB and DS-UWB system corresponding varying SNR for different B. The system parameters T_d and L_c are 200 ns and 4 respectively. The total BW of all systems are similar, 6 GHz. A timing jitter of NRMSJ=0.01% is assumed to be present in the system. It is found that DS-MB-UWB system generally outperforms DS-UWB system. Additionally, it is observed that DS-MB-UWB system that employs more number of bands performs better. Note that increasing B does not improve BER performance proportionately. For example, the BER improvement from B=1 to 2 bands is higher compared to B=2 to 4 bands.

Similarly, the BER performance behavior can be explained from the perspective of energy capture. Figure 12 compares the achievable captured energy by DS-UWB and DS-MB-UWB system with different number of sub-bands B and varying NRMSJ. It can be shown that DS-MB-UWB is able to capture more energy than DS-UWB systems at all value of NRMSJ. Furthermore, the higher B becomes, the more energy can be captured. The reason is, as more sub-bands are employed, the sub-band BW becomes narrower. With reference to region 2 in Fig. 9, we are aware that systems with narrower BW perform better. When NRMSJ increases, the captured energy generally decreases. However, the observation that DS-MB-UWB with higher B captures more energy still holds, despite increasing NRMSJ. By employing more sub-bands, DS-MB-UWB system is able to capture more fractional energy, and thus have better BER performance.

4.4 Number of Combined Paths

With the presence of timing jitter, the energy capture capability of selective Rake (SRake) is degraded due to the mistiming of each template signal. Therefore, the BER perfor-

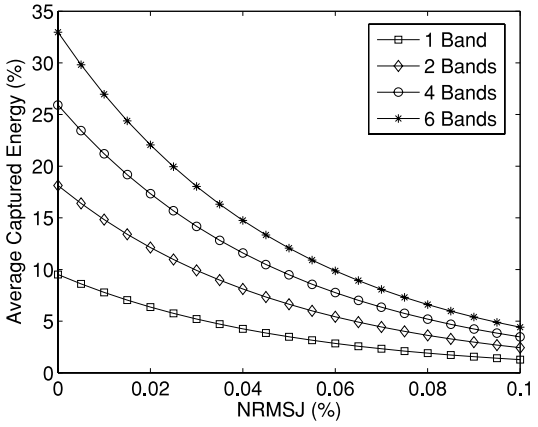

Fig. 12 Average captured energy vs. NRMSJ for DS-UWB and DS-MB-UWB systems. T_d=200 ns, L_c=4, BW=6 GHz, BPSK, Exp. decaying PDP, C=10.

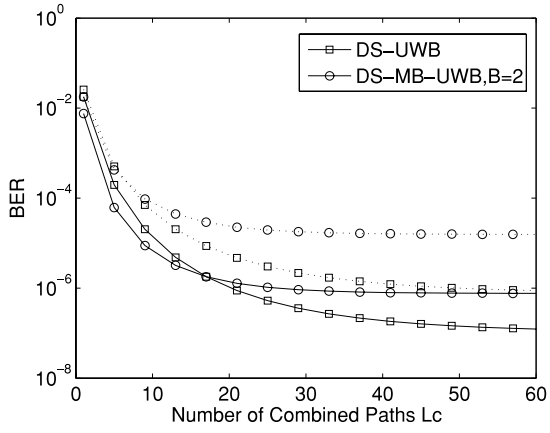

Fig. 13 BER performance vs. L_c for DS-UWB and DS-MB-UWB systems. T_d=200 ns, BW=2 GHz, SNR=12 dB, BPSK, Exp. Decaying PDP C=10. Solid line: NRMSJ=0.01%, Dotted line: NRMSJ=0.05%.

mance will be affected. According to (21), the system BER performance depends on the number of SRake combined paths L_c and pulse autocorrelation function in the presence of timing jitter. The relationship between L_c, flat and exponentially decaying PDP can be given in (19) and (20), respectively.

Figure 13 presents impact of timing jitter from the aspect of BER performance for DS-UWB and DS-MB-UWB systems for various L_c. We can see for NRMSJ=0.01% at lower L_c, DS-MB-UWB performs slightly better. As NRMSJ increases to 0.05%, the BER performance between two systems at low L_c becomes similar. On the other hand, as L_c becomes higher, DS-UWB is found to perform better than DS-MB-UWB system generally. In other words, the advantage of DS-MB-UWB system from the perspective of SRake combined paths can be obtained at low L_c, where lower system complexity can be achieved. At higher L_c, DS-UWB system is able to capture more energy comparatively and thus, having better BER performance.

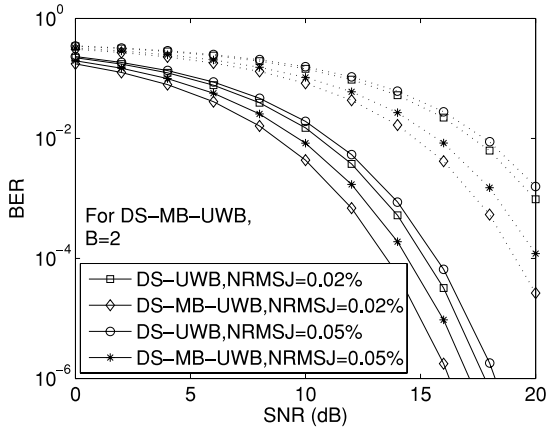

Fig. 14 BER performance vs. SNR for DS-UWB and DS-MB-UWB systems for different multipath channels. T_d=200 ns, L_c=4, BW=4 GHz, BPSK. Solid line: Exp. Decaying PDP, C=10, Dotted line: Flat PDP.

4.5 Types of Channel

The channel type determines the pattern of energy distribution along the multipath and thus affects the system BER performance. The relationship between energy capture and multipath channel with different PDP can be determined in (19) for flat PDP and (20) for exponentially decaying PDP. The amount of captured energy determines the BER performance as described in (21).

Figure 14 presents the impact of timing jitter on DS-UWB and DS-MB-UWB system performance corresponding two types of multipath channel with Rayleigh distributed fading: with exponential decaying PDP and flat PDP. We found that both systems generally perform better in channel with exponential decaying PDP. This is reasonable because for exponential decaying PDP, the receiver is able to capture more energy at lower L_c. Additionally, we can see that DS-MB-UWB outperforms DS-UWB system in both channels. The degradation due to timing jitter is found to be similar for both types of channels.

4.6 M-ary Signaling Levels

The employment of M-ary signaling provides advantages such as conserving bandwidth or increasing data rate at the expense of system performance. However, with the presence of timing jitter, the system performance of MPSK signals will be further degraded. Here symbol error rate (SER) is used to quantify the system performance as described in (21). Figure 15 shows the SER performance of using several levels of M-ary signals. Even without the presence of timing jitter, as M-ary level increases, the SER performance is degraded. The presence of timing jitter further degrades the SER performance. In Fig. 15, NRMSJ of 5% degrades SNR of approximately 2 dB for M-ary levels of 2, 4 and 8 at SER=10^{-6}.

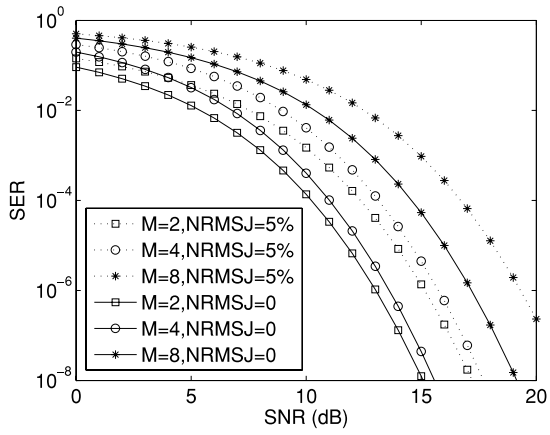

Fig. 15 SER performance vs. SNR for MPSK DS-UWB system. T_d=100 ns, L_c=8, BW=1 GHz. Exp. Decaying PDP, C=10.

5. Conclusion

In this paper, we address the impact of timing jitter on both DS-UWB and DS-MB-UWB systems with a selective Rake receiver over AWGN and multipath channel with Rayleigh distributed fading with different power delay profiles. A theoretical framework is developed to analyze the system performance in timing jitter environment. We found that the DS-MB-UWB system has better system performance in timing jitter environment due to its capability to have higher fractional energy capture in the correlation process. Also, the impact of timing jitter is analyzed according to system parameters such as pulse waveform, center frequency, bandwidth, data modulation, number of combined paths in Rake receiver, channel type and M-ary signaling level. With the presence of timing jitter, the amount of energy able to be captured by the receiver decreases considerably, thus degrading system performance. Potential future works includes the consideration of self interference and multi-user in the analysis.

Acknowledgment

This work is supported in part by the Grant-in-Aid for scientific research (No. 16560328), International Communication Foundation and Okawa Foundation.

References

[1] D. Porcino and W. Hirt, "Ultra-wideband radio technology: Potential and challenges ahead," IEEE Commun. Mag., vol.41, no.7, pp.66–74, July 2003.
[2] J. Foerster, E. Green, S. Somayazulu, and D. Leeper, "Ultra-wideband technology for short- or medium-range wireless communications," Intel Technology Journal, vol.5, no.2, May 2001.
[3] Federal Communications Commission, "First Report and Order, Revision of Part No.15," April 2002.
[4] Xtreme Spectrum Inc., "A tutorial in ultra-wideband technology," submission to IEEE P802.15 Working Group, March 2000.
[5] M.Z. Win and R.A. Scholtz, "Characterization of ultra-wideband wireless indoor channels: A communication-theoretic view," IEEE J. Sel. Areas Commun., vol.20, pp.1613–1627, Dec. 2002.
[6] J.R. Foerster, "The performance of a direct-sequence spread ultra wideband system in the presence of multipath, narrowband interference, and multiuser interference," Ultra Wideband Systems and Technologies, 2002. Digest of Papers. 2002 IEEE Conference on, pp.87–91, May 2002.
[7] R. Fisher, R. Kohno, M. McLaughlin, and M. Welborn, "DS-UWB physical layer submission to 802.15 task group 3a," Available: http://grouper.ieee.org/groups/802/15/pub/04
[8] D. Kelly, S. Reinhardt, R. Stanley, and M. Einhorn, "PulseOn second generation timing chip: Enabling UWB through precise timing," Ultra Wideband Systems and Technologies, 2002. Digest of Papers. 2002 IEEE Conference on, pp.117–121, May 2002.
[9] D. Rowe, B. Pollack, J. Puller, W. Chon, P. Jett, J. Fullerton, and L. Larson, "A Si/SiGe HBT timing generator IC for high-bandwidth impulse radio applications," Proc. Custom Integrated Circuits 1999, pp.221–224, May 1999.
[10] S. Sasaki, T. Kusama, J. Zhou, S. Muramatsu, and H. Kikuchi, "Impact of narrowband interference and timing jitter in DS-UWB system," International Symposium on Wireless Personal Multimedia Communications (WPMC'03), session TA6-1, pp.V2-274–277, Oct. 2003.
[11] Z. Tian and G.B. Giannakis, "BER sensitivity to mistiming in ultra-wideband impulse radios—Part I: Nonrandom channels," IEEE Trans. Signal Process., vol.53, no.4, pp.1550–1560, April 2005.
[12] Z. Tian and G.B. Giannakis, "BER sensitivity to mistiming in ultra-wideband impulse radios—Part II: Fading channels," IEEE Trans. Signal Process., vol.53, no.5, pp.1897–1907, May 2005.
[13] Y. Yin, J.P. Fonseka, and I. Korn, "Sensitivity to timing errors in EGC and MRC techniques," IEEE Trans. Commun., vol.51, no.4, pp.530–534, April 2003.
[14] I. Guvenc and H. Arslan, "Performance evaluation of UWB systems in the presence of timing jitter," Ultra Wideband Systems and Technologies, 2003 IEEE Conference on, pp.136–141, Nov. 2003.
[15] W.M. Lovelace and J.K. Townsend, "The effects of timing jitter and tracking on the performance of impulse radio," IEEE J. Sel. Areas Commun., vol.20, pp.1646–1651, Dec. 2002.
[16] G.T.F. Abreu and R. Kohno, "Design of jitter-robust orthogonal pulses for UWB systems," IEEE GLOBECOM 2003, vol.22, no.1, pp.739–743, Dec. 2003.
[17] C.S. Sum, M.A Rahman, and S. Sasaki, "Impact of timing jitter on Rake reception of DS-UWB signal over AWGN and multipath environment," WirelessCOM 2005, pp.1225–1230, Maui, Hawaii, June 2005.
[18] J.G. Proakis, Digital Comunications, 4th ed., McGraw Hill, New York, 2001.
[19] M.Z. Win and R.A. Scholtz, "On the energy capture of ultrawide bandwidth signals in dense multipath environment," IEEE Commun. Lett., vol.2, pp.245–247, Sept. 1998.
[20] W. Xu and L.B. Milstein, "On the performance of multicarrier RAKE systems," IEEE Trans. Commun., vol.49, no.10, pp.1812–1823, Oct. 2001.
[21] M.A. Rahman, S. Sasaki, J. Chou, S. Muramatsu, and H. Kikuchi, "Evaluation of selective Rake receiver in direct sequence ultra wideband communications in the presence of interference," Int. Workshop on Ultra Wideband Systems and Technologies 2004, pp.221–225, May 2004.
[22] M.Z. Win and R.A. Scholtz, "Impulse radio: How it works," IEEE Commun. Lett., vol.2, no.2, pp.36–38, Feb. 1998.
[23] J. Zhang, T.D. Abhayapala, and R.A. Kennedy, "Performance of ultra-wideband correlator receiver using Gaussian monocycles," ICC 2003, Communications, IEEE International Conference on, vol.26, no.1, pp.2192–2196, May 2003.
[24] M.A. Rahman, S. Sasaki, J. Zhou, and H. Kikuchi, "On Rake reception of ultra wideband signals over multipath channels from energy

capture perspective," IEICE Trans. Fundamentals, vol.E88-A, no.9, pp.2339–2349, Sept. 2005.
[25] Tektronix Jitter and Timing Analysis Reference Guide, "Understanding and characterizing timing jitter," Available: www.tektronix.com
[26] M.Z. Win, G. Chrisikos, and N.R. Sollenberger, "Performance of Rake reception in dense multipath channels: Implications of spreading bandwidth and selection diversity order," IEEE J. Sel. Areas Commun., vol.18, pp.1516–1525, Aug. 2000.

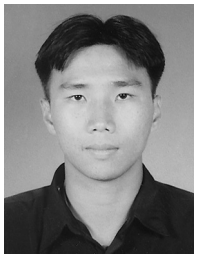

Chin Sean Sum received his Bachelor's degree in Electrical Engineering (EE) in May 2000 from University of Technology Malaysia (UTM), Johor, Malaysia. He then continued his research in sub-millimeter wave propagation and received his Master's degree in July 2002 from the same university. From April 2003, he is attached with Niigata University, Niigata, Japan as a Japanese Government (Monbukagakusho) scholar, where later in October 2003 he entered the Department of Electrical and Electronic Engineering as a research student. From April 2004 to present, he is working towards his Doctoral degree in the same university. His research interests include Ultra Wideband Communications, Communication Theory, Timing Jitter in Communication Systems and Multiband Communications etc. He is a student member of the IEEE.

Shigenobu Sasaki received B.E., M.E. and Ph.D. degrees from Nagaoka University of Technology, Nagaoka, Japan, in 1987, 1989 and 1993, respectively. Since 1992, he has been with Niigata University, where he is now an Associate Professor in the Department of Electrical and Electronic Engineering. From 1999 to 2000, he was a visiting scholar at the Department of Electrical and Computer Engineering, University of California, San Diego. Since 2003, he has been with the UWB technology institute, National Institute of Information and Communication Technology (NICT) as an expert researcher. His research interests are in the area of digital communications with special emphasis on spread spectrum communication systems, ultra-wideband communication systems and wireless communications. He is a member of the IEEE and SITA.

Hisakazu Kikuchi received the B.E. and M.E. degrees from Niigata University in 1974 and 1976, respectively, and Dr. Eng. degree from Tokyo Institute of Technology in 1988.From 1976 to 1979 he worked at Information Processing Systems Laboratory, Fujitsu Ltd., Tokyo. Since 1979 he has been with Niigata University, where he is a professor of electrical engineering. He was a visiting scholar at Electrical Engineering Department, University of California, Los Angeles during a year of 1992 to 1993. He holds a visiting professorship at Chongqing University of Posts and Telecommunications, China, since 2002. His research interests are in the areas of image/video processing and digital signal processing as well as ultra wideband systems. Dr. Kikuchi is a member of ITE (Institute of Image Information and Television Engineers), IIEEJ (Institute of Image Electronics Engineers of Japan), JSIAM (Japan Society for Industrial and Applied Mathematics), RISP (Research Institute of Signal Processing), IEEE, and SPIE. He served the chair of Circuits and Systems Group, IEICE, in 2000 and the general chair of Digital Signal Processing Symposium, IEICE, in 1988 and Karuizawa Workshop on Circuits and Systems, IEICE, in 1996.